Supplementary materials: Vibrational Coupling to Epsilon-Near-Zero Waveguide Modes.

Thomas G. Folland[1], Guanyu Lu[1], A. Bruncz[1,2], J. Ryan Nolen[3], Marko Tadjer[4] and Joshua D. Caldwell[1]

1. Department of Mechanical Engineering, Vanderbilt University, Nashville, TN, USA, 37212

2. Department of Physics, University of Alabama in Huntsville, Huntsville, AL, USA, 35899

3. Interdisciplinary Materials Science, Vanderbilt University, Nashville, TN, USA, 37212

4. US Naval Research Laboratory, Washington, DC 20375, United States of America

*josh.caldwell@vanderbilt.edu

1. Determining mode properties using numerical simulations

To determine the properties of the resonant modes that were observed in the highest aspect ratio 4H-SiC gratings (h=24μm), we employed electromagnetic simulations, as shown in Fig. S1. For the narrowest period structure with Λ=5 μm (Fig. S1 a/b), numerical simulations reproduce the experimental results for both field orientations. The simulated electric field profiles for the four lowest frequency modes in the E_x (TM) polarization (Fig. S1 i-iv), are all anti-symmetric across the gap. with a series of nodes oriented vertically downwards into the grating. Each progressive resonance exhibits an increase in the number of nodes (6, 7 and 8 for Fig. 2 i, iii, and iv, respectively). The feature at frequency 836 cm^{-1}, Fig. S1 ii, is not associated with a resonant mode (hence the similarities with Fig. 2iii), but instead arises from absorption from a zone-folded LO phonon in 4H-SiC[1], one of the unusual features of the vertical orientation of the field in these structures[2-3]. Finally, the absorption observed outside the Reststrahlen band is associated with waveguide modes concentrated inside the SiC, which has an extremely high index of refraction (up to n~20) at these frequencies due to the proximity to the strong absorption from the TO phonon[4]. In all, these simulations illustrate that the SiC grating forms a metal-insulator-metal TM polaritonic waveguide[5], and the vertical height of the grating forms a cavity resonator, consistent with earlier results in noble metals[6-8]. These waves show remarkably strong absorption at various frequencies across the entire Reststrahlen band, with a maximum absorption of 80% and Q~92 observed at 883 cm^{-1}, comparable with that achieved in many SPhP nanoantennas[3, 9-11]. However, unlike SPhP-based nanoantennas, in these HAG devices discussed here, the electromagnetic fields are not localized only at the corners of the structure, instead being distributed in the gap between adjacent grating teeth. This enables the modes to have a strong spatial overlap with local dipoles, such as molecular vibrational resonances, thereby providing further motivation to use these structures for liquid-based sensing modalities.

Whilst the plasmon polariton resonances occurring in HAG structures have been studied in prior work[6-8, 12-13], modes stimulated with E_y (TE) polarization have not been discussed. The electromagnetic fields associated with the three modes for the Λ=5μm grating (Fig. S1 vi-vii) are a series of standing-wave resonances within the cavity formed by the grating. These field profiles are consistent with the formation of TE waveguide modes, with a wavelength λ~2×h~50μm for the lowest order wave, much longer than that of light in free space (approx.. 4.2x longer). This corresponds to an effective index ($n_{eff} = \lambda_0/\lambda$ where λ_0 is the free space wavelength), of less than one. Traditional dielectric and polaritonic waveguide modes typically have an $n_{eff}>>1$, but $n_{eff}<<1$ can occur under certain conditions in metal-insulator-metal waveguides. As the waveguide mode approaches the cutoff frequency, n_{eff} of the waveguide mode drops to zero, also reducing the effective dielectric constant to zero. This leads to a significant enhancement of the electric field, as has been well studied in past work on epsilon near zero modes[5, 14-16]. Field enhancement can also be observed in our simulations - the peak electromagnetic field in the gap is stronger for the l=1 (by a factor of 20%) compared with the l=3 resonance. The fundamental TE mode at 957 cm^{-1} exhibits Q~108 and ~65% absorption, giving it properties comparable to those induced with TM polarization (absorption of 80% and Q~92). Enhancement of the local electric fields in both polarizations demonstrates that HAGs offer different types of waveguide modes that can be exploited for field enhanced sensing, among other applications.

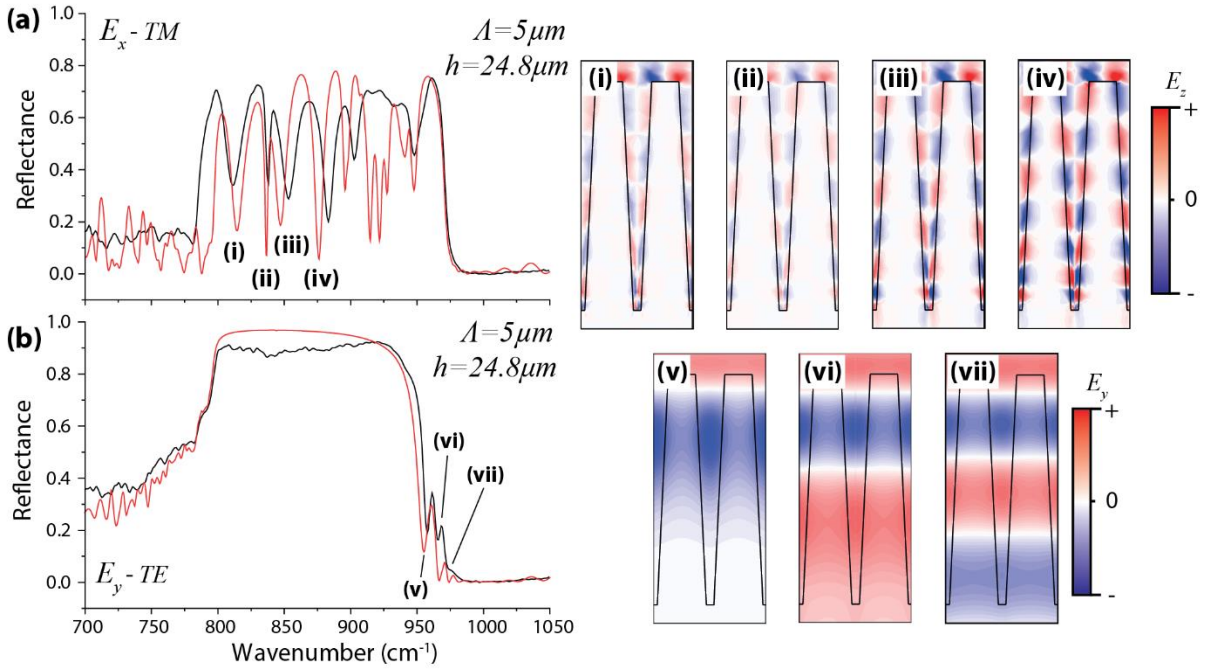

Figure S1. Waveguide modes in deep-etched SiC gratings. (a)/(b) shows TM/TE FTIR spectra for a grating of Λ=5 μm compared with numerical calculations. (i)-(vii) show the corresponding field profiles

2. Mode Lifetime of TE waveguide modes

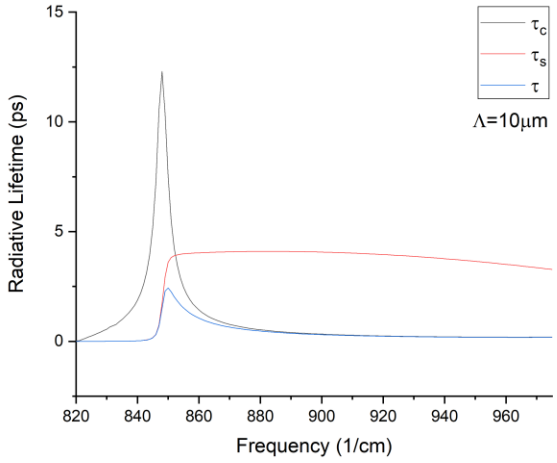

Figure S2. Mode lifetime (τ) and contribution from the cavity τ_c and mode loss τ_s for the Λ=10μm, h=24.8μm grating

3. Mode spectrum for h=11.5μm grating.

In the main text we primarily discuss the mode spectrum of the deepest (h=24.8μm) grating. However, similar properties can be measured for the shallower, h=11.5μm gratings, and the same general physics applies. For example, shorter gratings still support TE waveguide modes, albeit with fewer resonances due to the limited length of the cavity (Fig. S1). These modes show similar tuning, albeit with lower

quality factors and absorption depths. As such, height becomes a means to tune the frequency of TE waveguide modes, in addition to grating pitch.

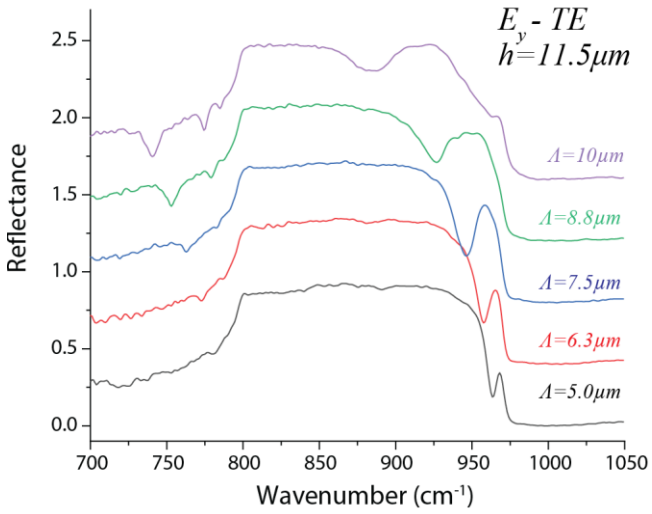

Figure S3. TE waveguide modes in a h=11.5μm grating. Fewer modes are observed than in Fig 2, due to the shallower depth of the grating.

4. Comparison of spectra in liquid environments

In addition to the studies of the TE modes in HAG structures, we also performed a comparative analysis with TM and grating waveguide modes. Through comparison of the IR reflectance spectra of the grating (solid lines) and unpatterned region (dashed lines) in different working liquids, the influence of the ENZ waveguide interactions with the liquid can be ascertained (Fig. S4 b-d). In the absence of a liquid, the grating resonances are clearly observable for both shallow and deep grating structures through the BaF_2 cover glass, similar to the results presented in Fig. 1-3. Upon submersion in acetone, the spectra for both the shallow ($h = 0.8\mu m$, Fig. S4b), and deep gratings ($h = 24.8\mu m$, Fig. S4c/d) develop multiple additional absorption bands that can be attributed to either polaritons, or absorption bands in the liquid. Whilst the polaritonic resonances are red-shifted due to the change in the local index when compared to their spectral location in air, the general features of the spectra are still present. The shifting of the modes suggests that these grating structures could also be attractive for index-based sensing in anhydrous environments. To assess the sensitivity to refractive index we can examine the shift in frequencies for (1) the TM mode in the shallow grating, and (2) the TE modes in the deep grating structures. Based on the 47 cm^{-1} spectral shift of the lowest frequency TM mode in the shallow grating, and 50 cm^{-1} shift of the lowest frequency TE mode in the deep grating, we estimate (assuming $n_{acetone}$ ~1.4[17]) a tuning sensitivity of 118 cm^{-1}/RIU and 125 cm^{-1}/RIU respectively. As the resolution of most commercial FTIR spectrometers is limited to a range 0.1-0.5 cm^{-1} we can argue that the minimum detectable change in index is on the order of 8×10^{-4} to 4×10^{-3}, comparable to past work using a prism to couple to SiC SPhPs[18]. This suggests that while there may be advantages to the HAG structures for index sensing, the advances are minor in comparison to index sensitivities in visible plasmonic systems. In water, despite the strong IR absorption, polaritonic resonances are still observed in both shallow and deep gratings. For shallow gratings the lines are significantly broadened in aqueous environments (from 15 cm^{-1} to ~40 cm^{-1} for the mode at ~884 cm^{-1}). However, for the HAG gratings we actually observe an enhanced optical signal from the grating structures vs the 'control' measurement. This is because much of the electromagnetic energy is actually stored within the low-loss SiC grating teeth, which increases the propagation length in water.

This alludes to the possibility of using SPhP structures to get longer optical path lengths in highly attenuating media. However, the resonances in such structures are also broadened, which makes it unclear if a HAG outperforms its shallow counterpart.

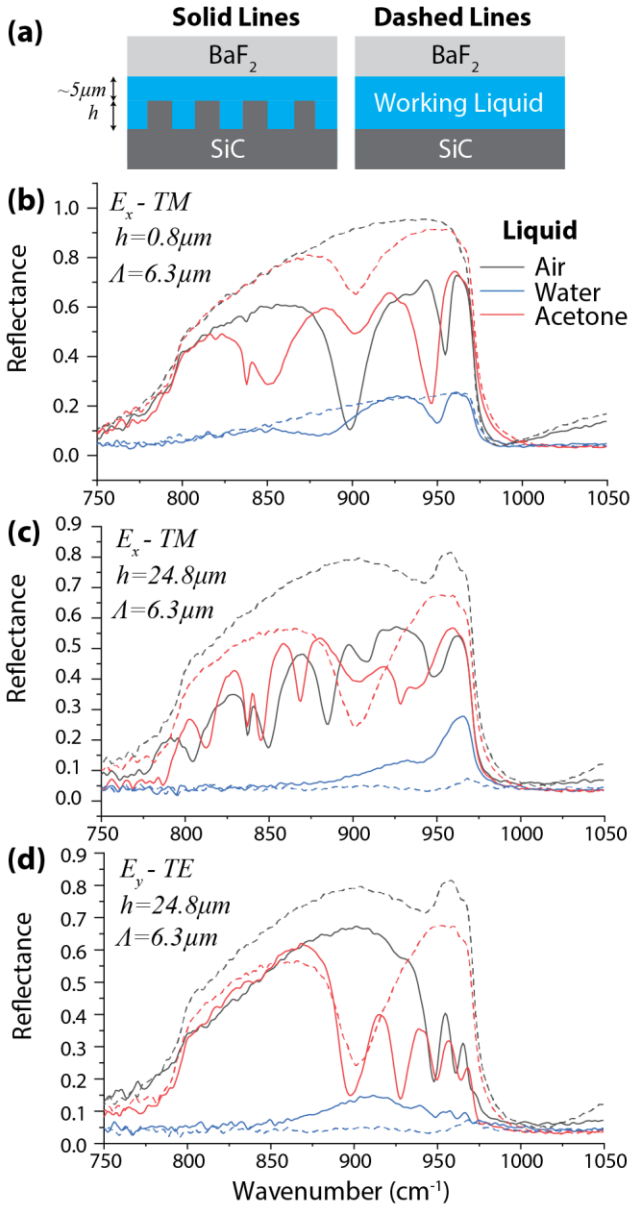

Fig. S4. Influence of liquid environment on grating resonances. A schematic of the experimental setup is shown in (a). FTIR reflectance spectra are shown in (b) and (c) for a shallow and deep grating respectively, with the electric field polarized along E_x, launching polariton modes. In (d) the we show reflectance spectra the deep grating with the electric field aligned along E_y, launching TE 'slab' waveguide modes.

5. Spectra of common organic solvents and resonance tuning

In order to determine the best candidates for sensing and strong coupling experiments, we performed FTIR spectroscopy of various solvents for the gratings in this paper. We find that whilst toluene and

acetone present very weak absorption bands, both cyclohexane and IPA present relatively strong vibrational bands for analysis in sensing experiments

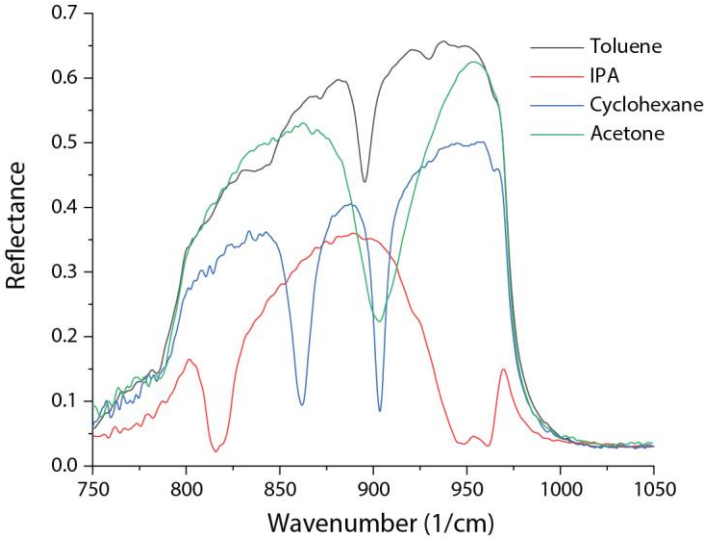

Fig S5. Infrared spectra of solvents taken in the liquid cell next to the gratings (following the process of Fig. 3)

In order to tune the resonance of the Λ=6.49μm grating in a different solvent to the vibrational band of cyclohexane we use a mixture of IPA and toluene. We find that a 1:1 ratio of toluene and IPA produces an appropriate modal overlap, as shown in Fig. S5

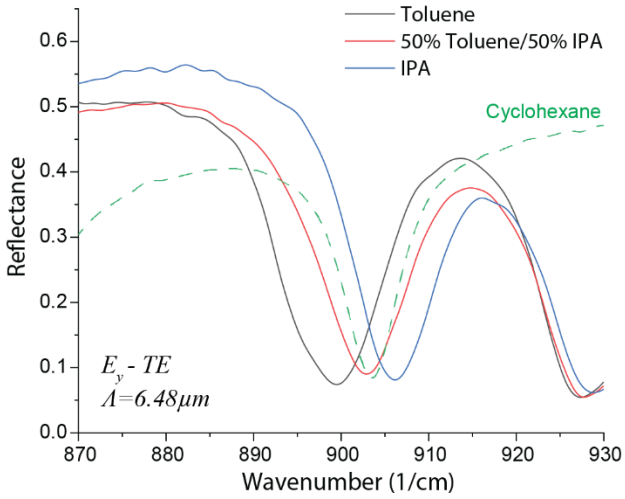

Figure S6. Mode tuning using different solvents for overlapping of cavity mode with the cyclohexane vibrational mode.

6. Strong coupling to TE waveguide modes

In order to provide further verification that we are observing a coherent coupling effect within our system, we can exploit the analytical model developed in the main text, inputting a complex dielectric function for the liquid as well as for the silicon carbide. To do so we generate a dielectric function for absorption in a polar liquid, using a simple Lorentz oscillator model:

$$\varepsilon(\omega) = \varepsilon_\infty + \frac{S}{\omega_0^2 - \omega^2 - i\gamma\omega}$$

ε_∞=1.56 is high frequency dielectric constant, S=1000cm^{-2} is oscillator strength, ω_0 = 903cm^{-1} is vibration energy and γ=8cm^{-1} is damping. By inputting this dielectric function into the analytical model of the main text we generate the dispersion relation and Q factors shown in Fig. S6. We consider four cases, the grating in air, the grating in a medium with index 1.225, the grating in a medium with a dispersive band at 903cm^{-1} (coincidence with the *l=1* mode) and a medium with a dispersive band at 939cm^{-1} (coincidence with the *l=3* mode). From the l=1 case the modes are significantly redshifted when moved into a medium with a higher refractive index. We also see that we can observe a fairly significant mode splitting of 12cm^{-1} for the *l=1* mode when the vibrational band overlaps with this mode order. This compares favourably to the linewidths extracted from the Q factors, (16cm^{-1} and 9.9cm^{-1}) suggesting that it this damping we are on the cusp of a strongly coupled system. Meanwhile, when the vibrational band overlaps with the *l=3* mode, we observe both a weaker mode splitting of 9cm^{-1} which is unfavourable when compared with the broadened linewidths of 32.2cm^{-1} and 23.35cm^{-1}. As a result, this mode would manifest not as a coupled mode, with distinct peaks but as a broadened mode. This highlights the importance of the *l=1* mode for strong coupling

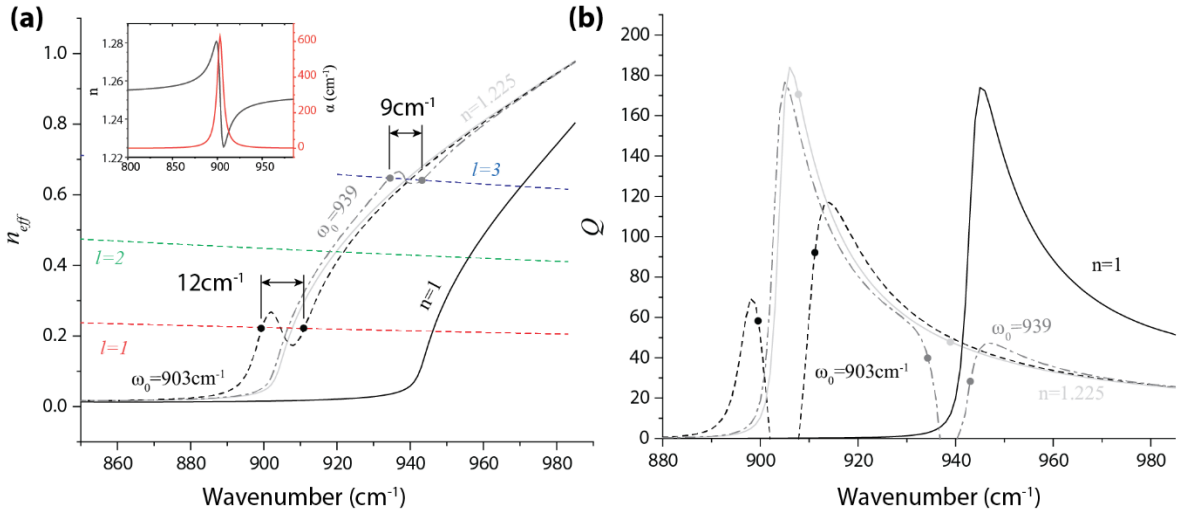

Figure S7. Analytical dispersion relation (a) and Q factors (b) for the TE polarized modes in a Λ=6.4μm grating. We find that the mode splitting is strongest for the *l=1* mode, and the Q factors for this mode are significantly higher, making this mode ideal for strong coupling. Inset shows dielectric model for the liquid when ω_0=903cm^{-1}.

7. Study of acetone-IPA mixtures

In order to assess if these gratings supported a SEIRA effect we studied the influence of small concentrations of IPA on the mode spectrum of the gratings. We consider both deep, and shallow grating modes, and as in the main text, compare the spectrum on the grating, to the control beside the grating. We find that even 2.5% of IPA in acetone produces a measurable dip in the spectrum taken next to the grating. However, on both shallow and deep gratings there is a minimal change in the grating spectrum, suggesting that there is minimal enhancement of absorption from these grating structures in this configuration.

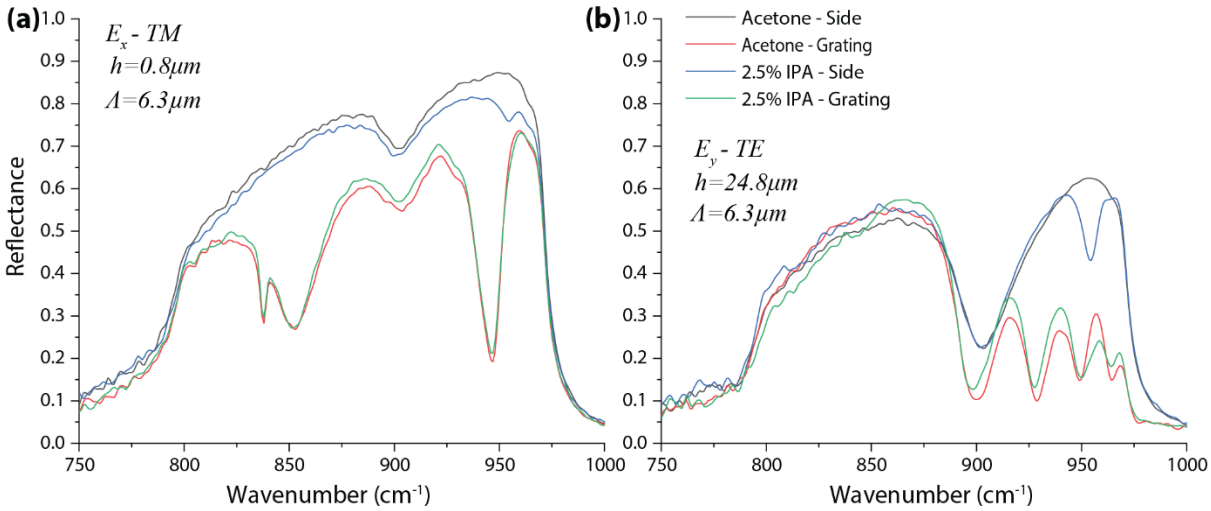

Figure S8. Absence of SEIRA for SiC gratings in acetone/IPA mixtures. Reflectance spectra for (a) shallow and (b) deep gratings in acetone and a 2.5% IPA mixture, compared against spectra next to the grating. For both shallow and deep gratings at 2.5% concentration the absorption line is strong and observable. However, there is minimal changes to the spectra on the gratings.

At higher concentrations of IPA for the shallow grating, we observe a separate IPA absorption peak superimposed on top of the grating mode. Spectra taken on the HAG grating indicate much stronger changes in mode frequency with concentration (Fig. S8 b). In order to extract the tuning range of the polariton mode we use a Lorentz fit to extract the mode positions for the modes indicated in Fig. S8 a/b, shown in Fig. 5c. Modes 1, 2 and 3 redshift with increasing IPA concentration, with a shift of 2.13cm^{-1}, 4.3cm^{-1} and 5.1 cm^{-1} respectively. Thus, we can say that the HAG structure shows much stronger sensitivity to the absorption band and the associated change in the dielectric constant of the ambient environment in the acetone IPA mix.

We also note that at high concentrations of IPA (45%) the mode closest to the IPA line appears to broaden into what could be multiple bands. Whilst in principle this could be strong coupling between the TE waveguide mode, and the IPA absorption line (as observed for cyclohexane), the splitting is not well defined. In order to study if this effect can be attributed to coupling, we can employ our analytical model for the waveguide modes, integrating a dielectric function for our acetone/IPA mixtures (see Fig. S7 for dielectric function). Upon the introduction of the IPA into the dispersion we observe a sigmoidal shape to the dispersion of the mode, which for the correct length cavity will produce a pronounced mode splitting. This contrasts with the much weaker absorption associated with the acetone, which does not produce a mode splitting effect due to its relatively weak and broad absorption. However, the high index of the liquid results in a suppression of the cavity reflectance *R*, resulting overdamping of the mode. This explains the lack of clear strong coupling in acetone-IPA mixtures.

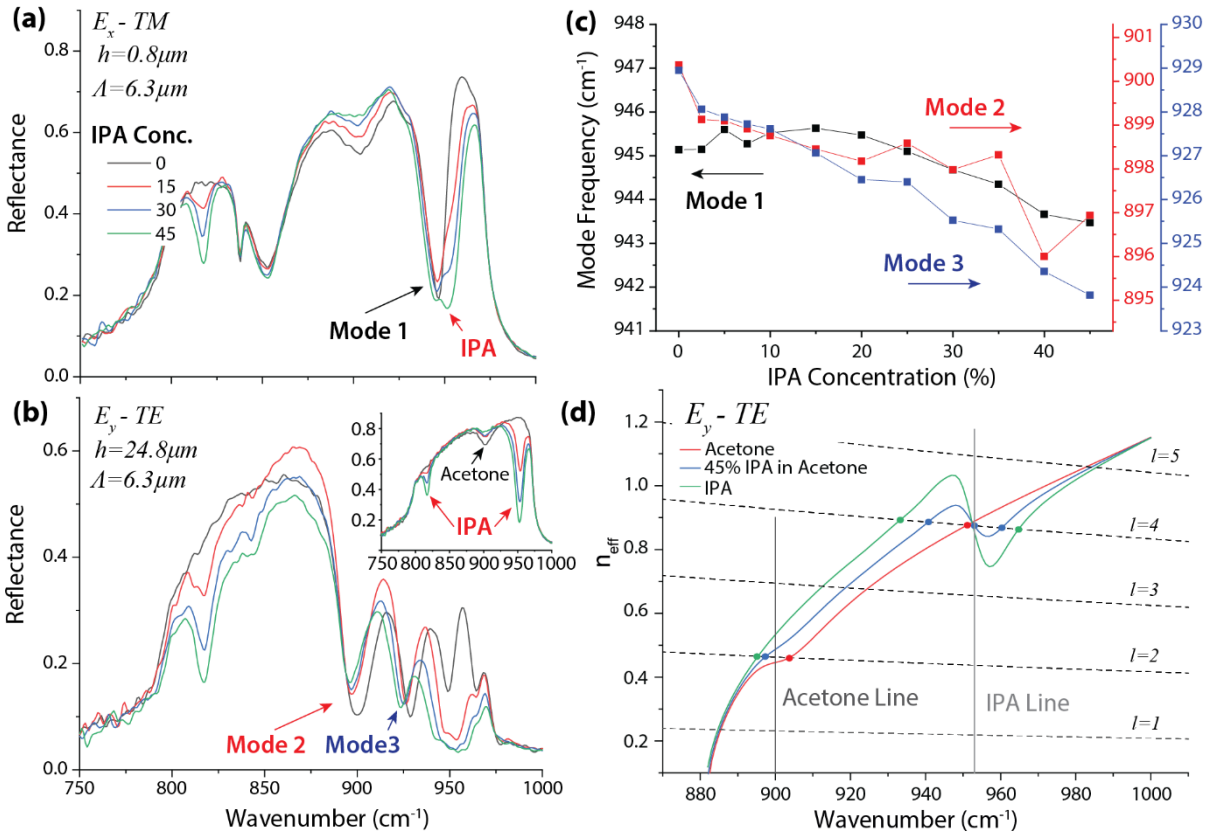

Figure S9. Grating enhanced spectroscopy of acetone-isopropyl alcohol mixtures. (a)/(b) shows the changes in the grating spectra as the concentration of IPA in acetone is increased for a shallow/deep grating respectively. (c) and (d) show the associated frequency tuning of the grating modes as the concentration is increased.

In order to use our analytical model for the waveguide modes we use a dielectric function for IPA reported in the literature[17]. We also use the same Lorentz model as above to generate a mode for acetone, where ε_∞=1.88, S=2016cm^{-2}, ω_0 = 900cm^{-1} and γ=20cm^{-1}. These values are chosen to be consistent with the amount of absorption observed off the gratings (inset Fig S9b). The dielectric function of mixtures is created by doing a weighted average of the two different materials, with all three shown in Fig S10.

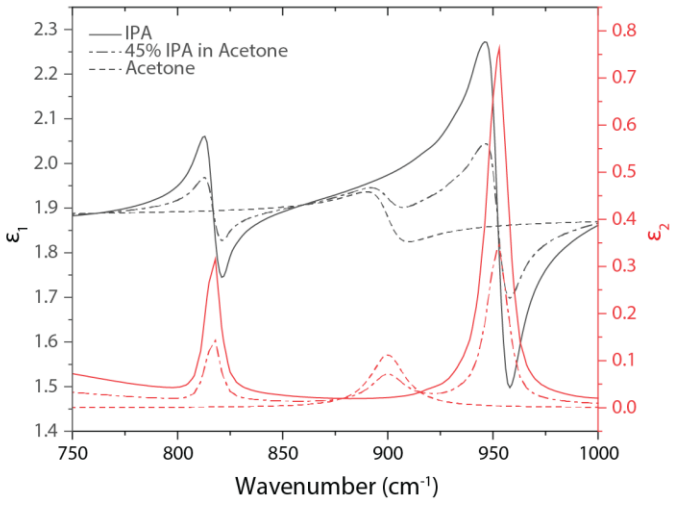

Figure S10. Dielectric function for IPA and acetone in the Reststrahlen band of 4H-SiC used in numerical calculations.

8. Determining cavity size in liquid cell

As described in the methods section, our liquid cell experiments produce a small gap between the grating under study and the piece of cover glass. This forms a reflective cavity, producing a series of etalon fringes in optical response, most clearly observed when the sample is in air (Fig. S11). By measuring the spacing of these fringes, we are able to estimate the height of the gap between the cover slip and sample. The frequency spacing of the fringes (Δf) 673 cm^{-1} (197 cm^{-1}), for h=0.8μm (h=24.8 μm) gratings is related to the size (L) of the cavity by $L=c/(2n\Delta f)$, where c is the speed of light and n is the index of the medium. This gives a height of the control cavity of 7.4μm for the grating with h=0.8 μm, and 25.4μm for the grating with h=24.8 μm.

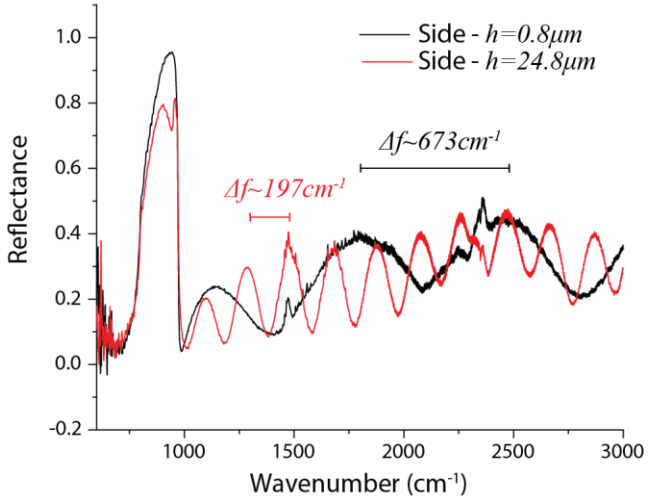

Figure S11. Fringe spacing outside the SiC Reststrahlen band. By analysing the mode spacing on the dry grating we can estimate the gap between the substrate and the BaF_2 cover.

References

1. Nakashima, S.; Harima, H., Raman Investigation of SiC Polytypes. *Physica Status Solidi Applied Research* **1997,** *162*, 39-64.
2. Gubbin, C. R.; Berte, R.; Meeker, M. A.; Giles, A. J.; Ellis, C. T.; Tischler, J. G.; Wheeler, V. D.; Maier, S. A.; Caldwell, J. D.; De Liberato, S., Hybrid longitudinal-transverse phonon polaritons. *Nature Communications* **2019,** *10* (1), 1682.
3. Caldwell, J. D.; Glembocki, O. J.; Sharac, N.; Long, J. P.; Owrutsky, J. O.; Vurgaftman, I.; Tischler, J. G.; Bezares, F. J.; Wheeler, V.; Bassim, N. D.; Shirey, L.; Francescato, Y.; Giannini, V.; Maier, S. A., Low-Loss, Extreme Sub-Diffraction Photon Confinement via Silicon Carbide Surface Phonon Polariton Nanopillar Resonators. *Nano Letters* **2013,** *13* (8), 3690-3697.
4. Schuller, J. A.; Zia, R.; Taubner, T.; Brongersma, M. L., Dielectric Metamaterials Based on Electric and Magnetic Resonances of Silicon Carbide Particles. *Physical Review Letters* **2007,** *99*, 107401.
5. Dionne, J. A.; Sweatlock, L. A.; Atwater, H. A.; Polman, A., Plasmon slot waveguides: Towards chip-scale propagation with subwavelength-scale localization. *Physical Review B* **2006,** *73* (3), 035407.

6. Sobnack, M. B.; Tan, W. C.; Wanstall, N. P.; Preist, T. W.; Sambles, J. R., Stationary Surface Plasmons on a Zero-Order Metal Grating. *Physical Review Letters* **1998,** *80* (25), 5667-5670.
7. Kreiter, M.; Mittler, S.; Knoll, W.; Sambles, J. R., Surface plasmon-related resonances on deep and asymmetric gold gratings. *Physical Review B* **2002,** *65* (12), 125415.
8. Liao, Y.-L.; Zhao, Y., Ultrabroadband absorber using a deep metallic grating with narrow slits. *Optics Communications* **2015,** *334*, 328-331.
9. Chen, Y.; Francescato, Y.; Caldwell, J. D.; Giannini, V.; Maß, T. W. W.; Glembocki, O. J.; Bezares, F. J.; Taubner, T.; Kasica, R.; Hong, M.; Maier, S. A., Spectral Tuning of Localized Surface Phonon Polariton Resonators for Low-Loss Mid-IR Applications. *ACS Photonics* **2014**, 140714145205007.
10. Caldwell, J. D.; Kretinin, A. V.; Chen, Y.; Giannini, V.; Fogler, M. M.; Francescato, Y.; Ellis, C. T.; Tischler, J. G.; Woods, C. R.; Giles, A. J.; Hong, M.; Watanabe, K.; Taniguchi, T.; Maier, S. A.; Novoselov, K. S., Sub-diffractional volume-confined polaritons in the natural hyperbolic material hexagonal boron nitride. *Nature Communications* **2014,** *5*, 5221.
11. Tamagnone, M.; Chaudhary, K.; Zhu, A.; Meretska, M.; Li, J.; Edgar, J. H.; Ambrosio, A.; Capasso, F., High quality factor polariton resonators using van der Waals materials. *arXiv preprint arXiv:1905.02177* **2019**.
12. Lyvers, D. P.; Moon, J.-M.; Kildishev, A. V.; Shalaev, V. M.; Wei, A., Gold Nanorod Arrays as Plasmonic Cavity Resonators. *ACS Nano* **2008,** *2* (12), 2569-2576.
13. Shukla, S.; Kim, K.-T.; Baev, A.; Yoon, Y. K.; Litchinitser, N. M.; Prasad, P. N., Fabrication and Characterization of Gold−Polymer Nanocomposite Plasmonic Nanoarrays in a Porous Alumina Template. *ACS Nano* **2010,** *4* (4), 2249-2255.
14. Vesseur, E. J. R.; Coenen, T.; Caglayan, H.; Engheta, N.; Polman, A., Experimental verification of n=0 structures for visible light. *Physical Review Letters* **2013,** *110*, 013902.
15. Liu, R.; Roberts, C. M.; Zhong, Y.; Podolskiy, V. A.; Wasserman, D., Epsilon-Near-Zero Photonics Wires. *ACS Photonics* **2016,** *3* (6), 1045-1052.
16. Alù, A.; Engheta, N., Dielectric sensing in $ϵ$-near-zero narrow waveguide channels. *Physical Review B* **2008,** *78* (4), 045102.
17. Sani, E.; Dell'Oro, A., Spectral optical constants of ethanol and isopropanol from ultraviolet to far infrared. *Optical Materials* **2016,** *60*, 137-141.
18. Neuner, B.; Korobkin, D.; Fietz, C.; Carole, D.; Ferro, G.; Shvets, G., Midinfrared Index Sensing of pL-Scale Analytes Based on Surface Phonon Polaritons in Silicon Carbide. *The Journal of Physical Chemistry C* **2010,** *114* (16), 7489-7491.